

Article

# Hotspot Temperature Prediction of Dry-Type Transformers Based on Particle Filter Optimization with Support Vector Regression

Yuanyuan Sun <sup>1,\*</sup>, Gongde Xu <sup>1</sup>, Na Li <sup>1</sup>, Kejun Li <sup>1</sup> , Yongliang Liang <sup>1</sup>, Hui Zhong <sup>1</sup>, Lina Zhang <sup>2</sup> and Ping Liu <sup>3</sup>

- <sup>1</sup> School of Electrical and Engineering, Shandong University, Jinan 250061, China; gongdexu@outlook.com (G.X.); lina2017@sdu.edu.cn (N.L.); lkjun@sdu.edu.cn (K.L.); liangyl@sdu.edu.cn (Y.L.); zhonghui@sdu.edu.cn (H.Z.)
- <sup>2</sup> Engineering Research & Design Department, CNOOC Research Institute, Beijing 100027, China; zhangln@cnooc.com.cn
- <sup>3</sup> CNOOC Energy Development of Equipment and Technology Co., Tianjin 300452, China; liuping5@cnooc.com.cn
- \* Correspondence: sunyy@sdu.edu.cn

**Abstract:** Both poor cooling methods and complex heat dissipation lead to prominent asymmetry in transformer temperature distribution. Both the operating life and load capacity of a power transformer are closely related to the winding hotspot temperature. Realizing accurate prediction of the hotspot temperature of transformer windings is the key to effectively preventing thermal faults in transformers, thus ensuring the reliable operation of transformers and accurately predicting transformer operating lifetimes. In this paper, a hot spot temperature prediction method is proposed based on the transformer operating parameters through the particle filter optimization support vector regression model. Based on the monitored transformer temperature, load rate, transformer cooling type, and ambient temperature, the hotspot temperature of a dry-type transformer can be predicted by a support vector regression method. The hyperparameters of the support vector regression are dynamically optimized here according to the particle filter to improve the optimization accuracy. The validity and accuracy of the proposed method are verified by comparing the proposed method with a traditional support vector regression method based on the real operating data of a 35 kV dry-type transformer.

**Keywords:** dry-type transformer; overheating fault; hotspot temperature prediction; online monitoring; support vector regression; particle filter



**Citation:** Sun, Y.; Xu, G.; Li, N.; Li, K.; Liang, Y.; Zhong, H.; Zhang, L.; Liu, P. Hotspot Temperature Prediction of Dry-Type Transformers Based on Particle Filter Optimization with Support Vector Regression. *Symmetry* **2021**, *13*, 1320. <https://doi.org/10.3390/sym13081320>

Academic Editor: Sergei Alexandrov

Received: 16 June 2021

Accepted: 17 July 2021

Published: 22 July 2021

**Publisher's Note:** MDPI stays neutral with regard to jurisdictional claims in published maps and institutional affiliations.



**Copyright:** © 2021 by the authors. Licensee MDPI, Basel, Switzerland. This article is an open access article distributed under the terms and conditions of the Creative Commons Attribution (CC BY) license (<https://creativecommons.org/licenses/by/4.0/>).

## 1. Introduction

Power systems in offshore oil and gas platforms are of great importance as they ensure the normal operation of platform and staff living activities. Dry-type transformers represent pivotal piece of equipment in the power system, and stable transformer operation is of great significance. Among all transformer faults, overheating faults are one of the most common types [1] and accelerate transformer insulation aging and can even lead to fires and explosions [2]. Due to the complex heat dissipation process of dry-type transformers, the asymmetry of transformer temperature distribution between phases is prominent. The temperature of phase-B winding is much higher than the other two-phase windings. Meanwhile, the asymmetry of the axial temperature distribution of the same phase is also worthy of attention, which affects the stable operation of the power system of offshore platforms seriously and factors strengthen the asymmetry problem of the distribution network. Hotspot temperature is an important indicator that characterizes a dry-type transformer's operating stat, where potential thermal faults can be predicted based on the temperature data. By avoiding possible overheating-related faults, the operating stability of dry-type transformers can be improved [3].

For dry-type transformers, there are mainly two methods to obtain hotspot temperature data, namely direct measurement and indirect calculation. With the development of online monitoring technology, resistance thermometer temperature sensors [4,5] are commonly embedded in transformer windings in transformer manufacturing. In addition, infrared thermal imaging technology is also used in transformer state monitoring, where the use of offline handheld imagers is most commonly used. Indirect calculation is based on theoretical and numerical calculations, including analytical, thermal network, and numerical analysis methods. An analytical method defines the hotspot temperature as the sum of the ambient temperature and the temperature rise of the hotspot temperature relative to the ambient temperature under a specific load [6]. A thermal network method uses thermoelectric analogy theory [7] to calculate the hotspot temperature of a transformer and a simplified equivalent circuit is used to illustrate the heat flow equation of the transformer. In the circuit, the current source represents the heat source caused by the transformer loss, the non-linear resistance represents the transformer cooling mode, and the ideal voltage source represents the transformer ambient temperature, where the solution of the transformer hotspot temperature can be converted into the solution of the node voltage of the circuit. Both a thermal network model based on the top oil temperature [8–10] and a thermal network model based on the bottom oil temperature [11] have been proposed; however, a dry-type transformer differs from an oil-immersed transformer in terms of the structure and heat dissipation type, and there is no thermal network model that is suitable for dry-type transformers. A numerical analysis method uses a finite element method [12] or a finite volume method to establish a 2D or 3D model [13,14] of the transformer. Furthermore, an electromagnetic thermally coupled model [15] or a fluid–solid coupled model [16,17] may be established to improve the accuracy of temperature estimation for transformers under an asymmetry condition. Although these methods have high accuracy and can obtain the temperature of each point inside a transformer, the long computation times of such methods makes them impossible for use in real-time online monitoring and analysis.

With the development of data analysis technology, intelligent learning methods such as the support vector machines [18–20], relevance vector machines [21], and kernel extreme learning machines [22,23] have been widely used for transformer fault diagnosis [24]. Transformer hotspot temperature prediction methods based on data analysis have also been proposed. Hotspot temperature prediction can be regarded as a problem involving finding the complex non-linear relationship between the hotspot temperature and the influencing factors. For hotspot temperature prediction with an oil-immersed transformer, the top oil temperature can be chosen as the prediction object. The temperatures of the measuring points and transformer operating parameters are chosen as the training data for the Kalman filter, neural network, support vector machine [25], and genetic programming method [26]; however, a dry-type transformer cannot use the top oil temperature as a prediction object and hotspot temperature prediction for dry-type transformers needs to be performed according to the actual heat generation mechanism. A support vector regression (SVR) [27] method is suitable for cases with a small set of sample data and meets the requirements for hotspot temperature prediction. Besides, the hyperparameters in SVR methods have a greater impact on the prediction results, and thus the elucidation of an appropriate optimization method to obtain optimal hyperparameters is of vital importance. K-fold cross-validation, grid methods, genetic algorithms [28] and particle swarm [29] methods are commonly used; however, in the cases with large data fluctuation, these methods cannot track newly observed data with the required speed and prediction accuracy.

To overcome the above disadvantages, in this paper, a particle filter optimization support vector regression method is proposed to predict the hotspot temperature of a dry-type transformer. The method can dynamically track the changes of hyperparameters. The hotspot temperature prediction model is a multi-input single-output problem in which the load rate, transformer ambient temperature, cooling type, and historical data of the hotspot temperature are used as inputs and the hotspot temperature of the dry-type transformer is

set as the output. The input data are obtained through an online temperature monitoring system. Since the measurement of the winding inner temperature is difficult due to the cast resin, an online infrared thermal imager can be used for online monitoring of the transformer temperature. The monitoring data of an existing Pt100 sensor may also be used to improve the monitoring accuracy of the transformer temperature. The installation position of the infrared thermal imager is determined by electromagnetic thermal multi-physics coupling analysis. Based on the data of a dry-type transformer temperature online monitoring system in an offshore oil and gas platform power system, the results of the particle filter optimization support vector regression method presented here are compared with a traditional support vector regression method for the hotspot temperature prediction with a dry-type transformer. The accuracy of the selected particle filter support vector regression method is also verified here.

## 2. Hotspot Temperature Prediction Model Based on the Particle Filter Support Vector Regression

### 2.1. The Input Parameters of the Prediction Model

The hotspot temperature of a dry-type transformer is affected by many operating factors, among which the four most important factors are the real-time load rate, the ambient temperature, the state of the cooling fan, and the historical hotspot temperature.

1. Load rate  $K$ : The copper loss generated by the primary and secondary windings during the operation of the dry-type transformer is the main heat source, and the winding resistance loss is proportional to the square of the load rate. When the load rate changes, the corresponding loss changes and consequently leads to temperature changes.
2. Ambient temperature  $T_a$ : Based on the principle of heat convection, the iron core and windings of dry-type transformers are directly in contact with air, and thermal convection is the main heat dissipation method. The ambient temperature affects the temperature of the dry-type transformer winding and consequently affects the hotspot temperature of the transformer.
3. Cooling fan status  $s_f$ : When the temperature of the transformer exceeds a certain limit, the cooling fan will be started in order to aid heat dissipation. Forced air cooling has a better heat dissipation effect than natural air flow. The temperature increase rate will be reduced when the fan is turned on.
4. Historical temperature  $T_s$ : The process of temperature variation has a time lagging characteristic. The current temperature is closely related to the temperature value of the previous period.

The four quantities, including the load rate  $K$ , ambient temperature  $T_a$ , cooling fan status  $s_f$ , and historical temperature  $T_s$ , are used here as inputs in the hotspot temperature prediction model  $x_i = [K, T_a, s_f, T_s]$ . The hotspot temperature at the next moment  $T_{hs}$  is the model output  $y_i = [T_{hs}]$ . This nonlinear problem is solved here by a particle filter optimization support vector regression method which is illustrated in the following section.

### 2.2. PF-SVR Hotspot Temperature Prediction Model

#### 2.2.1. Support Vector Regression Principle

Support vector regression (SVR) describes the application of support vectors in the field of functional regression. Similar with support vector machines, SVR methods are suitable for models with small sets of sample data. For the above hotspot temperature prediction, the training dataset is considered in the form of  $D = \{x_i, y_i\}_{i=1}^N$ , where  $x_i$  is a 4-dimensional input that includes the load rate, ambient temperature, cooling fan status, and historical hotspot temperature,  $y_i$  is the predicted output hotspot temperature, and  $N$  is the number of samples. The hotspot temperature prediction problem can be described as finding the functional relationship  $f$  between the output hotspot temperature  $y_i$  and input matrix  $x_i$ . This nonlinear relationship can be described by a data fitting

method. According to the principle of support vector regression, under linear conditions, the functional relationship can be described as follows:

$$y = f(x) = \mathbf{w}^T x + b \quad (1)$$

where  $\mathbf{w}$  and  $b$  are the parameters of the support vector regression model. The nonlinear relationship may be transformed into a linear relationship and a nonlinear mapping can be introduced as  $\Phi : R^l \rightarrow F$ , where  $F$  is the feature space of the mapping  $\Phi$ . The sample is mapped from the original space  $R^l$  to the high-dimensional space  $F$  while maintaining the simplicity of the expressed relations. The prediction can be described as per Equation (2):

$$y = f(x) = \mathbf{w}^T \Phi(x) + b \quad (2)$$

By adjusting the values of  $\mathbf{w}$  and  $b$ , the target loss function is minimized based on the training set  $D$  through the support vector regression model. The  $\varepsilon$ -insensitive loss function of the optimization model can be described as follows:

$$l = \begin{cases} 0, & |y - f(x)| \leq \varepsilon \\ |y - f(x)| - \varepsilon, & \text{others} \end{cases} \quad (3)$$

The  $\varepsilon$ -insensitive loss function is defined as the difference between the predicted output and the actual value, which is approximated to be zero when  $l$  is less than  $\varepsilon$ . When  $l$  is greater than  $\varepsilon$ , the relaxation variables  $\zeta$  and  $\zeta^*$  are introduced to represent the error, where  $\zeta$  represents the positive error and  $\zeta^*$  represents the negative error. The objective loss function and constraints in the SVR model can be expressed as per Equation (4):

$$\begin{aligned} \min_{\mathbf{w}, \zeta, \zeta^*} J(\mathbf{w}, \zeta, \zeta^*) &= \frac{1}{2} \|\mathbf{w}\|^2 + C \sum_{i=1}^n (\zeta + \zeta^*) \\ \text{s.t.} \begin{cases} y_i - \mathbf{w} \cdot \Phi(x_i) - b \leq \varepsilon + \zeta_i \\ \mathbf{w} \cdot \Phi(x_i) + b - y_i \leq \varepsilon + \zeta_i^* \\ \zeta_i, \zeta_i^* \geq 0 \end{cases} & \quad i = 1, \dots, N \end{aligned} \quad (4)$$

$\|\mathbf{w}\|^2$  is the confidence risk, which is related to the generalization ability of the regression model;  $\sum_{i=1}^n (\zeta + \zeta^*)$  is the empirical risk, representing the overall error of the regression model for the training data set; and parameter  $C$  is the compromise value of confidence risk and empirical risk. The SVR method has the advantages of minimizing structural risks and finding a globally optimal solution.

The Lagrange duality method may be used to optimize the solution as shown in Equation (5):

$$\hat{y} = \mathbf{w} \cdot \Phi(x) + b = \sum_{i=1}^N \hat{\alpha}^* K(x_i, x) + b \quad (5)$$

where  $\hat{\alpha}^*$  is the Lagrange multiplier in the optimization problem and  $K(x_i, x)$  is a kernel function, where any positive semidefinite function  $K$  can be used as a kernel function. This can be written in the following form:

$$K(x_i, x) = \Phi(x_i) \cdot \Phi(x) \quad (6)$$

A Gaussian kernel function is used in the SVR model.

$$K(x_1, x_2) = \exp\left(-\frac{\|x_1 - x_2\|^2}{\sigma^2}\right) \quad (7)$$

### 2.2.2. Particle Filter Principle

A particle filtering (PF) method is a sequential importance sampling method that is used to realize the model parameters that are dynamically adapted with the test data. For the established state space model, the distribution of parameters  $p(z_1)$ ,  $p(z_1 | z_{n-1})$ , and  $p(x_n | z_n)$  is known. Suppose that a time series of observation  $X_{n-1} = (x_1, x_2, \dots, x_{n-1})$  has been obtained and that  $p(z_n | X_{n-1})$  has been estimated. A new observation  $x_n$  is obtained such that the known estimation  $z_n$  can be corrected through  $x_n$ , and the new observation can be used to continuously modify the known estimation.

For any state, Equations (8) and (9) exist.

$$x(t) = f(x(t-1), u(t), w(t)) \quad (8)$$

$$z(t) = h(x(t), e(t)) \quad (9)$$

where  $x(t)$  is the state at time  $t$ ;  $u(t)$  is a control variable;  $w(t)$  and  $e(t)$  are the model noise and observation noise, respectively; and  $z(t)$  is the observation variable. Equation (8) is the state transition equation and Equation (9) is the observation equation.

According to Bayesian theory, the estimation problem can be converted to construct the probability density function  $p(x_k | z_{1:k})$  at state  $x_k$  and time  $k$  when the measured value at time  $k$  is known, which is shown in Equations (10) and (11):

$$p(x_k | z_{1:k-1}) = \int p(x_k | x_{k-1}) p(x_{k-1} | z_{1:k-1}) dx_{k-1} \quad (10)$$

$$p(x_k | z_{1:k}) = \frac{p(z_k | x_k) p(x_k | z_{1:k-1})}{p(z_k | z_{1:k-1})} \quad (11)$$

$$p(z_k | z_{1:k-1}) = \int p(z_k | x_k) p(x_k | z_{1:k-1}) dx_{k-1} \quad (12)$$

where  $p(x_{k-1} | z_{1:k-1})$  is the probability density function at time  $k-1$ ;  $p(x_k | z_{1:k-1})$  is the probability density function at time  $k$ ;  $p(x_k | x_{k-1})$  is determined by the system state equation;  $p(z_k | z_{1:k-1})$  is the normalization constant; and  $p(z_k | x_k)$  is the likelihood function.

In reality, it is usually difficult to solve for the optimal solution in most cases. Particle filtering provides a relatively easy and approximate optimal Bayesian solution. The core idea is that the posterior probability density function  $p(x_{0:k} | z_{1:k})$  of the state  $x_k$  at time  $k$  can be expressed by  $\{x_{0:k}^i, w_k^i\}_{i=1}^{N_s}$ , where  $w_k$  represents the weight and  $x_{0:k}$  represents the set of particles from time 0 to time  $k$ . The posterior probability density function of the true state of the system at time  $k$  can be expressed as follows:

$$p(x_{0:k} | z_{1:k}) \approx \sum_{i=1}^{N_s} \omega_k^i \delta(x_k - x_{0:k}^i) \quad (13)$$

where  $\delta$  is the Dirac function.

Assuming the importance density function  $q(x_{0:k} | z_{1:k})$  is used to determine  $\{x_{0:k}^i\}_{i=1}^{N_s}$ , the weights  $w_k^i$  should satisfy the following condition.

$$w_k^i \propto \frac{p(x_{0:k}^i | z_{1:k})}{q(x_{0:k}^i | z_{1:k})} \quad (14)$$

Since  $q(x_{0:k} | z_{1:k}) = q(x_k | x_{0:k}, z_{1:k}) q(x_{0:k-1} | z_{1:k-1})$ , the weight can be updated according to Equation (15).

$$w_k^i \propto w_{k-1}^i \frac{p(z_k | x_k^i) p(x_k^i | x_{k-1}^i)}{q(x_k^i | x_{k-1}^i, z_{1:k})} \quad (15)$$

The state vector  $x_k$  can be estimated by the sampling particles and related weights:

$$\hat{x}_k = \sum_{i=1}^{N_s} w_k^i x_k^i \quad (16)$$

### 2.2.3. SVR Parameter Optimization

It should be noted that the penalty coefficient  $C$ , the width of insensitive region  $\varepsilon$ , the kernel function parameters  $\sigma$ , and the correlations among these three parameters have a great impact on the complexity, generalization ability, and calculation speed of a SVR-based model. The value of the penalty coefficient  $C$  should be neither too small nor too large. If it is too small, then the modeling process will feature under-learning, and if it is too large then the modeling process will feature over-learning. Similarly, if the width of the insensitive region  $\varepsilon$  is too large, this will simultaneously reduce the calculation burden and learning accuracy. If the kernel function parameter  $\sigma$  is too small, the accuracy of the regression model will be poor; however, if  $\sigma$  is too large, the model will have a weak generalization ability. Consequently, the values of the three parameters ( $C$ ,  $\varepsilon$ , and  $\sigma$ ) need to be comprehensively considered in order to produce a good optimization result when using a SVR-based model.

$K$ -fold cross-validation is a common method for selecting SVR parameters. The parameter space is subdivided into several continuous cells and a discrete parameter set is selected for each cell, indicating a combination of parameter values. The training data are randomly divided into  $k$  mutually exclusive subsets of equal size and the regression function with the given parameter set is obtained using  $k - 1$  subsets, where the performance of the remaining subset is then tested. The same process is repeated  $k$  times with each subset being tested once. The average performance index over  $k$  trials represents an estimation of the expected generalization error obtained using a specific parameter set. The parameter set with the best performance can finally be obtained by repeating the above process for different parameter sets; however, as the parameter space size and the number of partition subsets increase, the computational burden also increases.

Some intelligent optimization algorithms are already used to optimize the SVR parameters, such as genetic algorithms and particle swarm optimization algorithms. First, the input and output datasets are divided into training and test subsets, and then the best parameter values of the model are determined based on the training data. In each search iteration, the model parameters are updated by the optimization algorithm to predict the output. The prediction error is calculated and verified until the iteration convergence criteria are met. The optimal parameter value of the model can thus be found based on the test dataset; however, the optimal parameters obtained this way are determined by the training data and remain to be fixed after the training process. If the data of the test subset are significantly different from the training data, the accuracy of the model is not optimal as the parameters of the SVR cannot be adjusted dynamically based on the new input and output data. As such, the elucidation of an optimal method to realize dynamic updates and optimization for SVR parameters is the key point of interest.

### 2.2.4. PF-SVR Optimization Method

The model parameters obtained by a PS-SVR method can be dynamically adapted with test data. If a SVR method based on the initial parameters cannot derive the required fitting performance for the test data, the particle filter (PF) will correct the SVR model until the model can meet the accuracy requirements. In order to predict the output at time instant  $k + 1$ , the SVR parameters at time instant  $k$  must first be estimated by PF. The estimation process includes the prediction and update stages. In the prediction step, the measured values from the beginning to time instant  $k - 1$  are input into the historical dataset, while the SVR parameters are predicted based on the historical data. When a new measured value is obtained at time  $k$ , the PF updates the SVR parameters at time  $k + 1$ .

based on the new data. The updated parameter is used to predict the new output at time  $k + 1$  and the new parameters at time  $k$  are also sent to the PF for the next iteration.

The estimation steps of the PF-SVR method are illustrated as follows and the flowchart is shown in Figure 1:

1. Particle initialization of the particle filter. The optimal SVR hyperparameters  $x_0$  at the initial time are obtained through the cross-validation and the range of the number of particles  $N_s$  is set to be 300 to 500. The initial particle set is set to be  $\{x_0^i = x_0, \omega_0^i = 1/N_s\}, i = 1, \dots, N_s$ .
2. Prediction model updating. When  $k = 1, 2, \dots$ , the particle set is recorded as  $\{x_{k-1}^i, \omega_{k-1}^i\}, i = 1, \dots, N_s$ .

- Perform particle resampling and particle drift operation on the particle set  $\{x_{k-1}^i, \omega_{k-1}^i\}, i = 1, \dots, N_s$  in order to obtain a new particle set  $(x_{k-1}^i, 1/N_s)$ .
- Perform a small random drift for each particle as follows:

$$\hat{x}_k^i = x_{k-1}^i + u_{k-1}^i \tag{17}$$

- Update the particle weight by measuring the possibility function value of  $z_k$  and the predicted value of  $\hat{x}_k^i$  at each state as follows:

$$\hat{\omega}_k^i \propto \omega_{k-1}^i p(y_k | \hat{x}_k^i) \tag{18}$$

- Perform weight normalization as follows:

$$\omega_{k-1}^i = \omega_{k-1}^i / \sum_{j=1}^{N_s} \omega_{k-1}^j \tag{19}$$

- Eliminate particles with lower weights, copy particles with higher weights, and regenerate new random particles as per  $\{x_k^i, \omega_k^i\}, i = 1, \dots, N_s$ .
3. Output the prediction result and establish a prediction model based on each particle  $x_k^i$  in the new particle set to obtain the prediction  $\hat{y}_{k+1}^i = g(x_k^i, s_k)$  at time instant  $k + 1$ . The final prediction result is shown in Equation (20):

$$\hat{y}_{k+1} = \frac{1}{N_s} \sum_{i=1}^{N_s} \hat{y}_{k+1}^i \tag{20}$$

4. Update the prediction model and return to step (2).

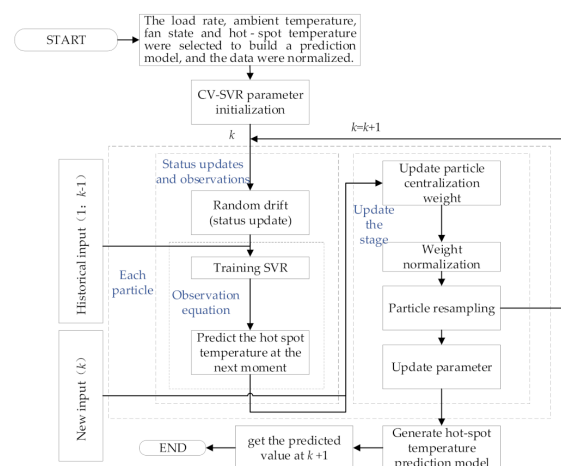


Figure 1. PF-SVR forecast flow chart.

### 3. Dry-Type Transformer Temperature Online Monitoring

An online temperature monitoring system of the dry-type transformer can be established to obtain the prediction model data. The position of the hotspot temperature cannot be determined with sufficient precision and only the area where the hotspot temperature exists can be roughly estimated. The Pt100 sensor is installed in a transformer for fixed-point monitoring and an infrared thermal imager is installed to obtain the winding surface temperature. These sensors together allow uninterrupted online monitoring of information regarding the real-time temperature, historical temperature, load current, fan status, and ambient temperature, thus enabling multi-parameter fusion, temperature trend analysis, overheating alarm support, and hotspot temperature prediction. Such a system allows one to track the latest temperature data and determine temperature abnormalities in real time. The specific features of such a system are the following:

1. Display and store the hotspot temperature of the three-phase winding and display and store the highest temperature in the monitoring area of the infrared thermal imager;
2. an overheat alarm threshold is set to the initial value and can be adjusted;
3. display the trend curve of historical temperature data and the initial value of historical time can be adjusted;
4. the hotspot temperature can be combined with the historical temperature, load current, ambient temperature, fan status, and other characteristics to comprehensively judge the transformer temperature status.

The advantages of online temperature monitoring can be summarized as follows:

1. Any continuous temperature changes of the transformer can be monitored, which is helpful for the long-term statistics and overall status assessment of a dry-type transformer;
2. From point detection to surface detection, the temperature images of the entire monitoring area can be obtained, and the hotspot temperature can be recorded;
3. The non-contact temperature sensor can be combined with an existing embedded temperature sensor, which does not affect the normal operation of the transformer;
4. Online temperature monitoring enables the measure of a large temperature range with a high monitoring accuracy. The temperature measurement range of infrared thermal imaging is generally  $-20\text{ }^{\circ}\text{C}$  to  $180\text{ }^{\circ}\text{C}$ , and the monitoring error is typically  $\pm 2\text{ }^{\circ}\text{C}$ .

#### 3.1. Analysis of Hotspot Temperature Location Based on Electromagnetic Thermal Coupled Model

The loss inside each point of a dry-type transformer is different, resulting in different heat source properties. The heat loss calculation will affect the results of field temperature analyses. In order to accurately calculate temperature fields and determine hotspot locations, this paper establishes an electromagnetic thermally coupled model to analyze the internal temperature distribution of a dry-type transformer. First, a 3D finite element electromagnetic field model is established with corresponding material properties for different components. An external circuit is used to realize the coupled field–circuit calculation to obtain each part of the loss. The core and winding losses obtained by the analysis are coupled to the temperature field analysis with a heat source input for temperature analysis. The corresponding heat dissipation coefficient for convection is set to obtain the temperature distribution for each region of interest. The rates of temperature change are far smaller than the rates of change for the electromagnetic field. The temperature of the transformer is calculated by indirect coupling. The coupling method is shown in Figure 2 and the coupling steps are given as follows:

1. A field–circuit coupled finite element model is established where the electric and magnetic fields are coupled, and the core loss and winding loss may then be analyzed;
2. The dry-type transformer losses obtained from the simulation are compared with theoretical values to verify the accuracy of the model;
3. An indirect coupling method is used to couple the electromagnetic and temperature fields, in which the loss is used as the transmission medium to realize coupling and the distribution of the temperature field of each part is analyzed;

4. Different load rates and ambient temperatures are set, and the transformer temperature distribution and hotspot locations in different states are analyzed;
5. The temperature distribution is solved iteratively.

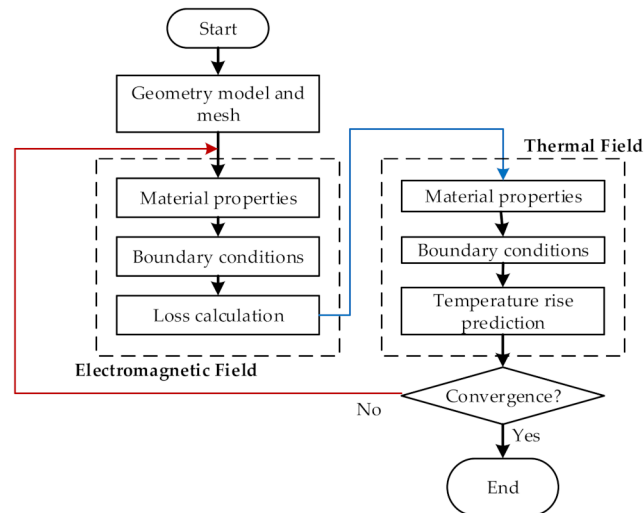


**Figure 2.** Iterative flowchart of the indirect coupling calculation.

Based on the actual parameters of a transformer on an offshore platform, a three-dimensional finite element electromagnetic simulation model was established as shown in Figure 3.

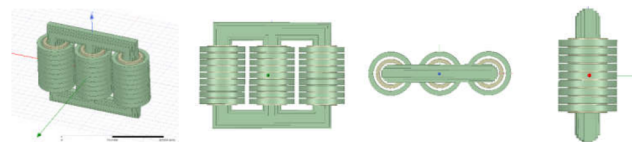


**Figure 3.** 3D finite element simulation model of a transformer.

Mesh division will directly affect the simulation calculation results. The finer the mesh division is, the higher the accuracy of the analysis; however, a larger computer memory capacity is also required as a result. The mesh results for this work are shown in Figure 4.

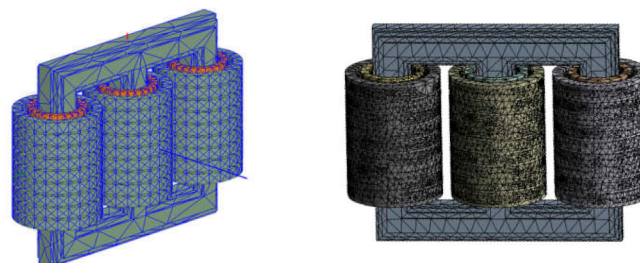


**Figure 4.** Mesh result for the electromagnetic field (left) and temperature field (right).

By using the ANSYS Workbench simulation platform, the core and winding losses obtained by a Maxwell electromagnetic field simulation were coupled in a steady-state thermal field simulation software package to determine the temperature field distribution. Combined with the ambient temperature information recorded by the offshore platform, the ambient temperature was set to 22 °C and the temperature distributions under different working conditions were simulated as shown in Figures 5–8 for the temperature distributions inside the transformer under various rated working conditions. It can be seen from

the distribution diagram that a hotspot temperature location appeared in the low-voltage winding. This is because the dry-type transformer mainly dissipates heat by natural air convection, and the internal heat dissipation methods are mainly heat conduction, convection, and radiation. Specifically, the core and winding are internal heat sources and the heat is transferred to a solid surface through the iron core and the winding by heat conduction. Air channels for heat dissipation exist between the windings in general and additionally between the low-voltage winding and the core. Due to the high current flowing through the low-voltage winding, the low-voltage winding generates more heat than the core and the high-voltage winding. Meanwhile, the heat dissipation effect is not optimal, so the temperature of the low-voltage winding is higher than the other two parts.

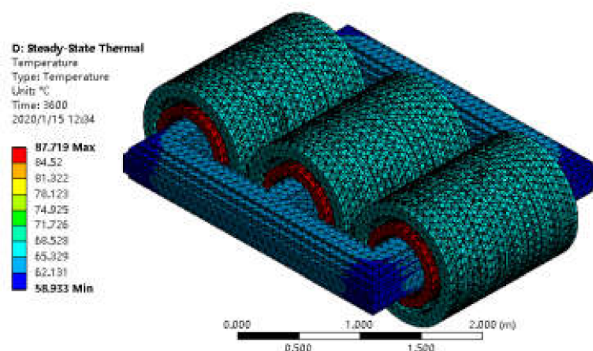


Figure 5. Overall temperature distribution of the transformer.

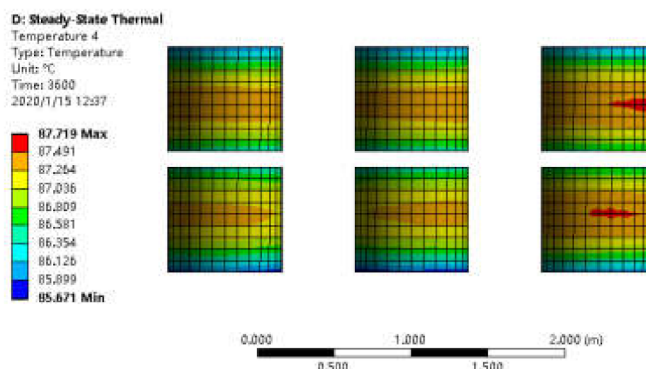


Figure 6. Low-voltage winding temperature distribution.

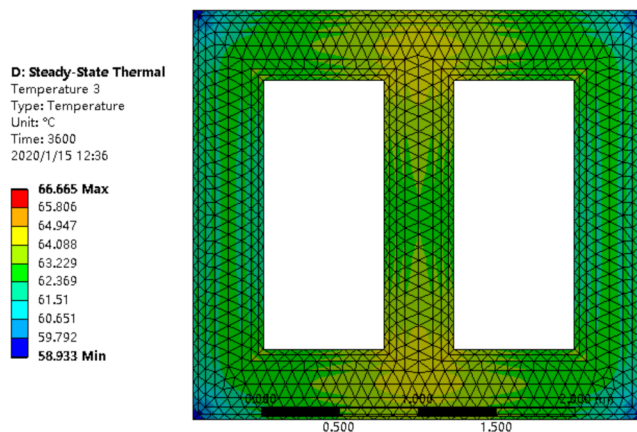
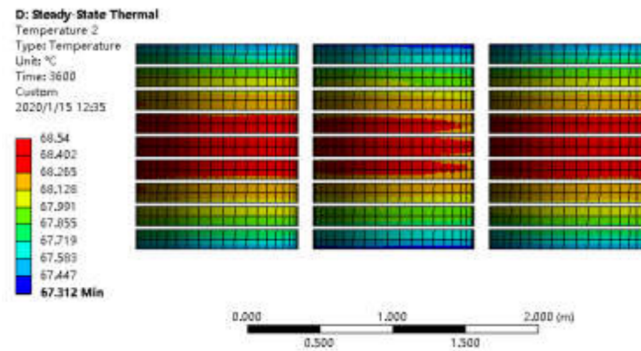


Figure 7. Core temperature distribution.



**Figure 8.** High-voltage winding temperature distribution.

It can be seen from the temperature distribution diagrams of the iron core, low-voltage winding, and high-voltage winding that the air is heated and then expands to move upward from the bottom area, which makes the air temperature in the bottom area lower. The temperature in the upper region is due to the improved heat dissipation conditions and as the nearby lower temperature causes the heat to gather in the middle region. This results in a hotspot appearing in the upper middle part of the transformer. Thus, the hotspot of the transformer was determined to be located in the upper half of the low-voltage winding, and the temperature of the middle phase (phase B) is higher than that of the other two phases.

In order to monitor the hotspot temperature, a temperature sensor should be installed in the upper half of the B-phase low-voltage winding. It is considered that there is an abnormal temperature if the temperature at this time exceeds the threshold.

### 3.2. Temperature Monitoring Based on Infrared Thermal Imager

In offshore oil and gas platform power systems, it is difficult to install an embedded temperature sensor in a dry-type transformer that has been put into operation; however, regarding non-contact sensors, infrared temperature sensors are more suitable, especially infrared thermal imagers, which can obtain visual temperature information optically and can intuitively observe the given temperature status. Such systems are widely used in power equipment fault monitoring. As a dry-type transformer does not feature an insulating oil package, the temperature of a high-voltage winding can be directly observed. Consequently, an infrared thermal imager was introduced to measure the temperature of the transformer. This paper is based on the original Pt100 temperature measurement sensor and the online infrared thermal imager was used to help determine the temperature status of the transformer.

#### 3.2.1. Principle of Infrared Thermal Imager

According to the Stefan–Boltzmann law of thermodynamics, the surface temperature of an object changes with the thermal power emitted by the object. An infrared thermal imager is based on this principle and measures the power of an object through the principle of radiation to obtain the surface temperature of the object, which reflects the status of the transformer as follows:

$$P = \varepsilon\delta T^4 \quad (21)$$

where  $P$  is the radiation power of the object;  $\varepsilon$  is the emissivity; and  $\delta$  is the Stefan–Boltzmann constant. The principle of infrared thermal imager is shown in Figure 9.

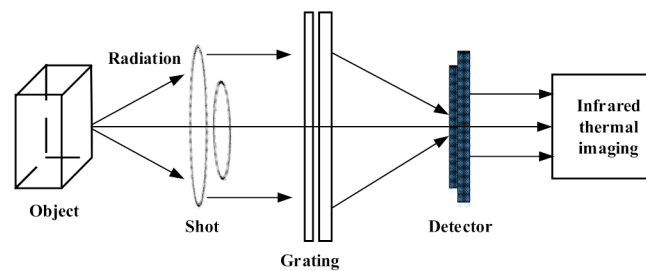


Figure 9. Infrared thermal imaging schematic.

### 3.2.2. Design of the Thermal Monitoring System

The infrared thermal imager temperature measurement design diagram is shown in Figure 9, which is composed of hardware and software. First, the infrared thermal imager obtains the temperature information of the dry-type transformer winding through the principle of thermal radiation and forms the temperature image and temperature information through internal processing. Then, through the data transmission interface, the hotspot temperature value is transmitted to the host computer for data analysis and processing, and the hotspot temperature value and temperature change trends are displayed for reference in operation and for use by maintenance personnel, as is shown in Figure 10.

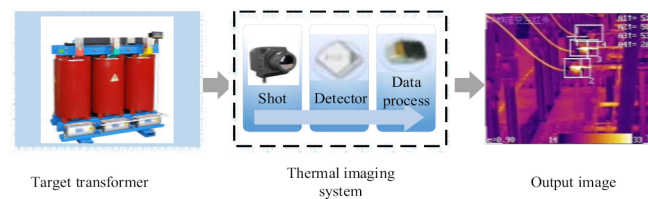


Figure 10. Infrared thermal imaging schematic.

The technical parameters of the infrared temperature sensor include the spectral response range, temperature measurement range, emissivity, and optical resolution, etc. Considering the monitoring accuracy and economy, this paper selected a DM20 network temperature measurement module as an online infrared thermal imager. As shown in Figure 11, the module has a small size and is easily integrated. Additionally, the module features a network interface, analog video interface, alarm interface, and RS485 interface. The temperature measurement range of the module is approximately  $-20\text{ }^{\circ}\text{C}$  to  $150\text{ }^{\circ}\text{C}$ . The temperature measurement error is  $\pm 2\%$ . The intended working environment temperature is approximately  $-15\text{ }^{\circ}\text{C}$  to  $65\text{ }^{\circ}\text{C}$  and the intended working environment humidity is  $\leq 95\%$ . Moreover, the modules meets the IEC68-2-6 standard for vibration testing and is suitable for installation at sea.



Figure 11. DM20 infrared thermal imager.

According to the analysis of the temperature field of the 35 kV dry-type transformer, the hotspot temperature of the B-phase (middle-phase) winding was slightly higher than that of the A- and C-phase windings. The hotspot temperature appeared in the upper half of the low-voltage winding and the winding temperature presented with a circumferential characteristic. The distribution was uniform; however, the low-voltage winding was located between the iron core and the high-voltage winding, which could not be directly observed by the infrared thermal imager. The heat transfer relationship between the high-voltage winding and the low-voltage winding is known. For the middle and upper parts of the high-voltage winding of the phase, we selected one side for easy installation as shown in Figure 12.

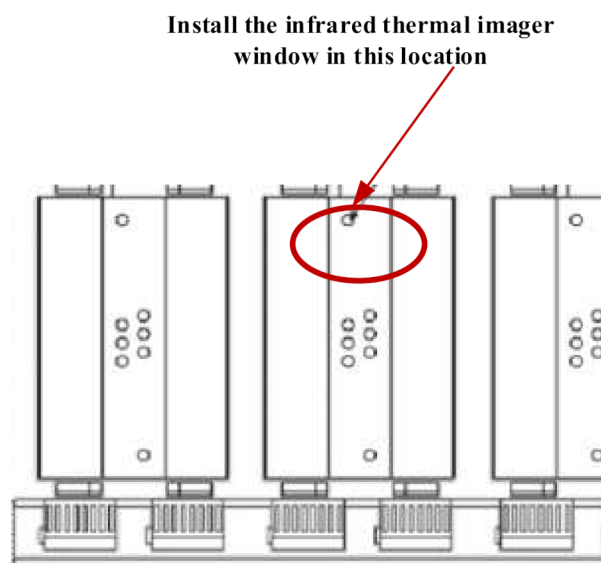


**Figure 12.** Schematic diagram of installation location.

#### 4. Results Analysis

The temperature sensor monitored the transformer temperature continuously and data were recorded every hour. The measured data obtained from a 35 kV dry-type transformer for use in an offshore oil and gas platform power system were used as the sample data for prediction. The transformer parameters are shown in Table 1. Figure 13 demonstrates data for the factor under consideration, including the historical hotspot temperature, ambient temperature, and load rate. Furthermore, the figure hints at the times at which the hotspot temperature exceeded 80 °C, fan turned on, and state changed from 0 to 1.

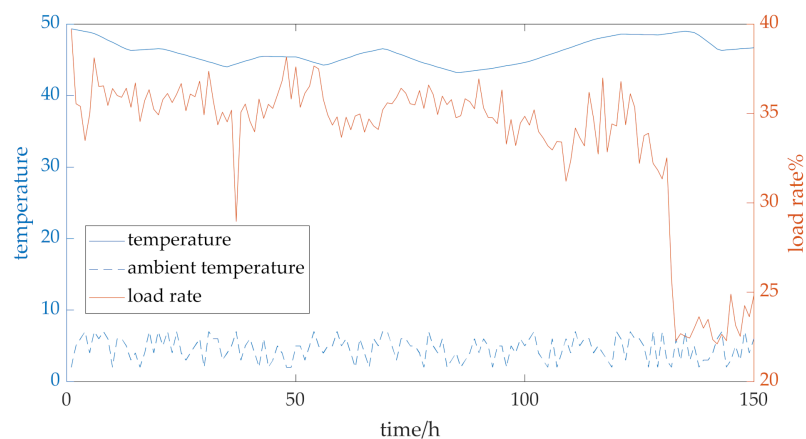
In this section, the Gaussian kernel function was chosen as the kernel function of the support vector regression algorithm. The initial value  $x_0$  ( $C$ ,  $\varepsilon$ ,  $\sigma$ ) of the parameter optimization in the particle filter algorithm was obtained by a 10-fold cross-validation method. The effect of the prediction method was evaluated by means of the root-mean-square error (RMSE), standard root-mean-square error (NRMSE), and mean absolute percentage error (MAPE). The indicator formulae are given below:

$$RMSE = \sqrt{\frac{1}{n} \sum_{i=1}^n (\hat{y}_i - y_i)^2} \quad (22)$$

where  $n$  is the number of samples,  $\hat{y}_i$  is the predicted value, and  $y_i$  is the actual measured value. The range of the RMSE was  $[0, +\infty)$ , where smaller values result in smaller errors and more accurate prediction.

**Table 1.** Electrical parameters of the transformer.

Type	Value	Type	Value
Model	PSCZ10-8000/6.3/35	Rated capacity	8000
Rated voltage/kV	6.3/35	Rated current/A	733/132
Phase number	3	Rated frequency/Hz	50
Group label	YNd11	Insulation class	F
Tapping range	$\pm 4 \times 2.5\%$	Rated load loss/W	40,400 (120 °C)
No-load loss/W	12,100		

**Figure 13.** Original data for the factors under consideration.

$$NRMSE = \sqrt{\frac{\sum_{i=1}^n (\hat{y}_i - y_i)^2}{\sum_{i=1}^n y_i}} \quad (23)$$

The range of the NRMSE was  $[0, +\infty)$ , where smaller values result in smaller errors and more accurate prediction.

$$MAPE = \frac{100\%}{n} \sum_{i=1}^n \left| \frac{\hat{y}_i - y_i}{y_i} \right| \quad (24)$$

In order to show the superiority of the PF-SVR prediction method, a traditional support vector regression algorithm was compared here. Fifty sets of data from January 2019 were selected. The input data included the ambient temperature, load rate, fan status, and historical hotspot temperature, and the output included the predicted temperature. The first 30 sets were used for training and the remaining 20 sets were used for testing.

Table 2 shows that the RMSE and NRMSE values of the PF-SVR model were smaller than those of the CV-SVR model. According to the definition of the three indicators, the smaller the error, the better the prediction effect, and as such the prediction of the PF-SVR model was better. It can be seen from Figure 14 that the hotspot temperature of the transformer was around 45 °C. On the one hand, the load rate of the transformer was low at this time. On the other hand, the ambient temperature in winter is low, and the transformer is safe and stable when operating in such conditions. The PF-SVR prediction results were better than CV-SVR as the PF-SVR method could adaptively update the model parameters according to new observation data. This made the model very robust to changes in data trends, while the CV-SVR model parameters were only optimized with the training data, and the prediction accuracy thus decreased accordingly.

**Table 2.** Comparative table of the prediction results.

	RMSE (°C)	NRMSE (°C <sup>1/2</sup> )	MAPE
CV-SVR	0.1147	0.1565	0.1645
PF-SVR	0.0812	0.1107	0.0876

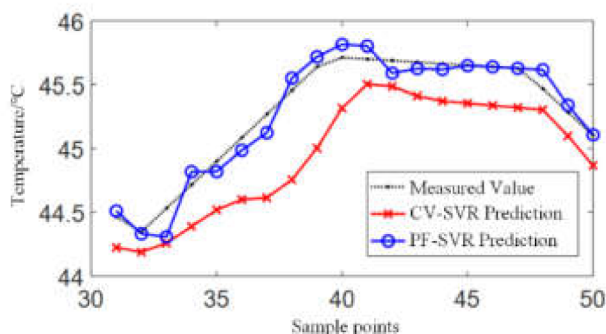


**Figure 14.** Forecast for the hotspot temperature with data from January in 2019.

The timespan of 50 sets of data was short and the ambient temperature changes were not obvious. Consequently, the data of other months were chosen to verify the proposed method. Figures 15 and 16 show the prediction results for April 2019 and July 2019, respectively. It can also be seen from Tables 3 and 4 that the PF-SVR results always maintained high prediction accuracy, while the CV-SVR prediction results fluctuated greatly. This is because when the training set data and the test set data are significantly different, the CV-SVR cannot update the optimal parameters of the SVR, consequently resulting in a decline in prediction performance.

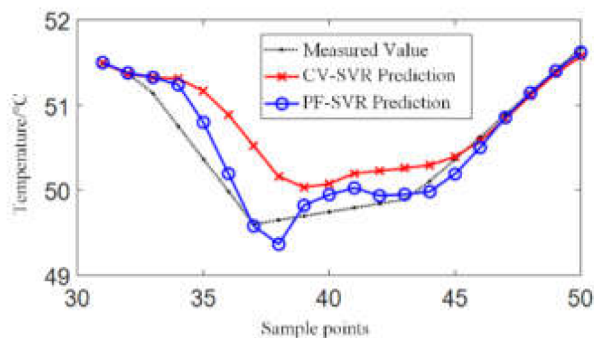


**Figure 15.** Forecast for the hotspot temperature with data from April in 2019.

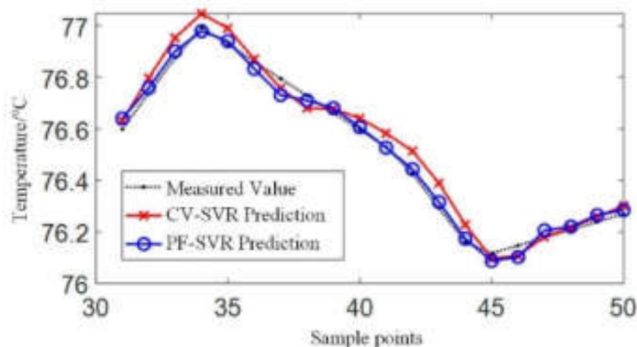


**Figure 16.** Forecast for the hotspot temperature with data from July in 2019.

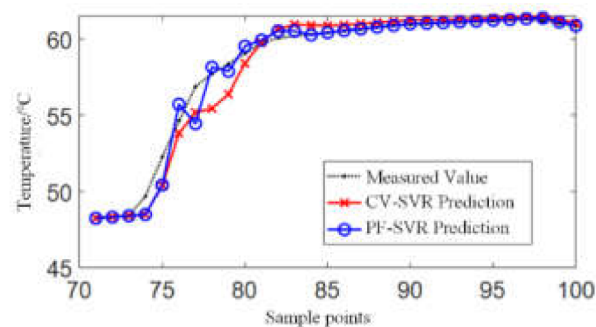
**Table 3.** Comparative table of the prediction results.

	RMSE (°C)	NRMSE (°C <sup>1/2</sup> )	MAPE
CV-SVR	0.1152	0.1687	0.1614
PF-SVR	0.0530	0.0776	0.0675

**Table 4.** Comparison table of prediction results.

	RMSE (°C)	NRMSE (°C <sup>1/2</sup> )	MAPE
CV-SVR	0.0632	0.1335	0.3035
PF-SVR	0.0338	0.0713	0.2635

In order to analyze the impact of training dataset size on the prediction results, another 100 datasets from December 2018 were selected. The first 70 sets of data were used for training and the other 30 sets were used for testing. It can be seen from Figure 17 that the PF-SVR model still maintained good prediction performance, and there were almost no differences between results when considering the 30 datasets used for training, so the prediction performance of the PF-SVR was thus less affected by the number of data in the training set. The prediction results of the CS-SVR model were also better, as increasing the training dataset size can improve prediction performance, which is also reflected in Table 5. Consequently, the performance of the CS-SVR model was greatly affected by the number of data in the training set.

**Figure 17.** Forecast for the hotspot temperature with data from December in 2019.**Table 5.** Comparison table of prediction results.

	RMSE (°C)	NRMSE (°C <sup>1/2</sup> )	MAPE
CV-SVR	0.0993	0.1853	1.0505
PF-SVR	0.0739	0.1469	0.5669

In order to test the versatility of the method considered here, another transformer with the same configuration was analyzed. The results are shown in Figure 18 and Table 6. It can be seen that the prediction results of the CV-SVR and PF-SVR models were better; however, the temperature tracking effect of the PF-SVR model was better.

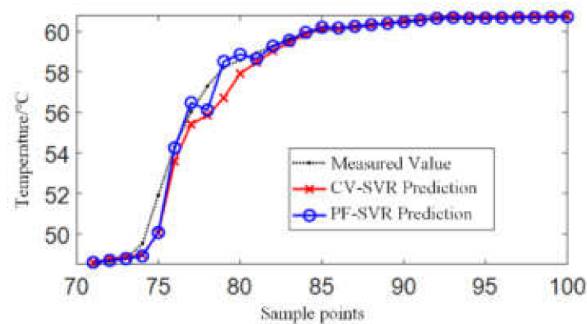


Figure 18. Hotspot temperature prediction for another transformer.

Table 6. Comparative table for the prediction results.

	RMSE (°C)	NRMSE (°C <sup>1/2</sup> )	MAPE
CV-SVR	0.0993	0.1853	1.0505
PF-SVR	0.0739	0.1469	0.5669

## 5. Conclusions

Based on the monitoring data of an online transformer temperature monitoring system, this paper has studied a hotspot temperature prediction method based on a particle filter support vector regression technique. The following conclusions have been obtained:

The online monitoring system, combining a Pt100 thermal resistance sensor and infrared thermal imager for temperature measurement, has realized non-contact monitoring of temperature. From point detection to surface detection, the temperature of the entire monitoring area can be obtained and hotspot locations can be viably determined. Continuous temperature changes are conducive to acquiring long-term statistics, and the system presented here is conducive to the overall status assessment of dry-type transformers.

The applicability of the support vector regression approach for hotspot temperature prediction was analyzed, and a particle filtering technique was used to optimize the parameters of the support vector regression method. The particle filter could dynamically track new observations and consequently provide optimal SVR parameters for the system.

Combined with the offshore platform monitoring load rate, ambient temperature, fan status, and historical hotspot temperature information, the PF-SVR model was used to predict hotspot temperatures. The proposed method was compared with a traditional SVR method in terms of the RMSE, NRMSE, and MAPE results. The results illustrate that the prediction accuracy of the PF-SVR model was higher. The analysis results are based on hotspot temperatures for several months, and the hotspot temperature of another transformer shows that the PF-SVR model was less affected by the number of training groups and is more suitable for the prediction of hotspot temperatures in dry-type transformers.

The significance of this article is mainly reflected in two aspects. On the one hand, hotspot temperature prediction for dry-type transformers provides an early warning system for transformer overheating, which helps to detect overheating faults in advance, consequently reducing the transformer failure rates and ensuring the stable operation of dry-type transformers. On the other hand, the hotspot temperature is an important condition that restricts the safe operation of a transformer and is an important factor that restricts the service life of a transformer. The research and determination of the hotspot temperature here provides a theoretical basis for research on the life of a transformer. In subsequent research, the relationship between the hotspot temperature and transformer lifetime will be considered to establish a remaining life calculation method to further guide the operation and maintenance of transformers.

**Author Contributions:** Conceptualization, Y.S. and N.L.; methodology, N.L.; software, G.X.; validation, H.Z., Y.S.; formal analysis, K.L.; investigation, G.X.; resources, Y.L., P.L. and L.Z.; writing—original draft preparation, N.L.; writing—review and editing, Y.S., G.X.; visualization, Y.L.; supervision, Y.S., K.L. All authors have read and agreed to the published version of the manuscript.

**Funding:** The work was supported by The National Key Research and Development Program of China under grant #2018YFB0904800.

**Data Availability Statement:** The data presented in this study are available on request from the corresponding author.

**Conflicts of Interest:** The authors declare no conflict of interest.

## References

1. Eslamian, M.; Vahidi, B.; Eslamian, A. Thermal analysis of cast resin dry-type transformers. *Energy Convers. Manag.* **2011**, *52*, 2479–2488. [[CrossRef](#)]
2. Rahimpour, E.; Azizian, D. Analysis of Temperature Distribution in Cast-resin Dry-type Transformers. *Electr. Eng.* **2007**, *89*, 301–309. [[CrossRef](#)]
3. Cha, C.; Kim, J.K.; Kweon, K.Y. Investigation of the thermal head effect in a power transformer. In Proceedings of the 2009 Transmission & Distribution Conference & Exposition: Asia and Pacific, Seoul, Korea, 26–30 October 2009; Volume 67, pp. 1–4. [[CrossRef](#)]
4. Wang, E.; Zhao, Z.; Cao, M. Multi Point Temperature Monitoring of Oil Immersed Transformer Based on Fiber Bragg Grating. *High Volt. Eng.* **2017**, *43*, 1543–1549. [[CrossRef](#)]
5. Zhao, Z.; Jiang, F.; Li, Y. Air-cooled Thermal Circuit Model and FBG Temperature Measurement of Transformer Winding. *High Volt. Eng.* **2017**, *43*, 3938–3943. [[CrossRef](#)]
6. Feng, D.; Wang, D.; Paul, J. Evaluation of Power Transformers' Effective Hot-Spot Factors by Thermal Modeling of Scrapped Units. *IEEE Trans. Power Deliv.* **2014**, *29*, 2077–2085. [[CrossRef](#)]
7. Swift, G.; Molinski, T.S.; Lehn, W. A fundamental approach to transformer thermal modeling-Part I: Theory and equivalent circuit. *IEEE Trans. Power Deliv.* **2001**, *16*, 171–175. [[CrossRef](#)]
8. Susa, D.; Nordman, H. A Simple Model for Calculating Transformer Hot-Spot Temperature. *IEEE Trans. Power Deliv.* **2009**, *24*, 1257–1265. [[CrossRef](#)]
9. Tang, W.; Wu, Q.; Richardson, Z.J. Equivalent heat circuit-based power transformer thermal model. *Electr. Power Appl. IEEE Proc.* **2002**, *149*, 87–92. [[CrossRef](#)]
10. Li, Y.; Liu, N.; Liang, Y. A Model of Load Capacity Assessment for Oil-immersed Transformer by Using Temperature Rise Characteristics. *Proc. CSEE* **2018**, *38*, 6737–6746. [[CrossRef](#)]
11. Elmoudi, A. Transformer windings hot spot temperature modeling and simulation. In Proceedings of the 2014 IEEE 27th Canadian Conference on Electrical and Computer Engineering (CCECE), Toronto, ON, Canada, 4–7 May 2014; pp. 1–5. [[CrossRef](#)]
12. Kang, Y.; Bai, B.; Guo, Y. Application of Field-Circuit Coupling Method of 3D Transient Finite Element Analysis for Large Power Transformers. *Trans. China Electrotech. Soc.* **2014**, *29*, 219–224. [[CrossRef](#)]
13. Li, L. A Novel Approach to Investigate the Hot-Spot Temperature Rise in Power Transformers. *IEEE Trans. Magn.* **2015**, *51*, 1–4. [[CrossRef](#)]
14. Santiseban, A.; Delgado, F.; Ortiz, A. Numerical Analysis of The Hot-Spot Temperature of a Power Transformer with Alternative Dielectric Liquids. *IEEE Trans. Dielectr. Electr. Insul.* **2017**, *24*, 3226–3235. [[CrossRef](#)]
15. Liao, C.; Ruan, J.; Liu, C. 3-D Coupled Electromagnetic-Fluid-Thermal Analysis of Oil-Immersed Triangular Wound Core Transformer. *IEEE Trans. Magn.* **2014**, *50*, 1–4. [[CrossRef](#)]
16. Ding, X.; Ning, W. Analysis of the Dry-type Transformer Temperature Field Based on Fluid-solid Coupling. In Proceedings of the 2012 Second International Conference on Instrumentation Measurement, Computer, Communication and Control, Harbin, China, 8–10 December 2012; pp. 520–523. [[CrossRef](#)]
17. Xu, Y.; Liu, F.; Qi, Y. Prediction of Winding Temperature in Power Transformers Based on Fluid Network. *High Volt. Eng.* **2017**, *43*, 1509–1517. [[CrossRef](#)]
18. Yang, Z.; Zhou, Q.; Wu, X.; Zhao, Z. A Novel Measuring Method of Interfacial Tension of Transformer Oil Combined PSO Optimized SVM and Multi Frequency Ultrasonic Technology. *IEEE Access* **2019**, *7*, 182624–182631. [[CrossRef](#)]
19. Cui, Y.; Ma, H.; Saha, T. Improvement of power transformer insulation diagnosis using oil characteristics data preprocessed by SMOTE Boost technique. *IEEE Trans. Dielectr. Electr. Insul.* **2014**, *21*, 2363–2373. [[CrossRef](#)]
20. Lu, P. Real-Time Monitoring of Temperature Rises of Energized Transformer Cores with Distributed Optical Fiber Sensors. *IEEE Trans. Power Deliv.* **2019**, *34*, 1588–1598. [[CrossRef](#)]
21. Khosravi, A.; Nahavandi, S.; Creighton, D.; Atiya, A.F. Comprehensive Review of Neural Network-Based Prediction Intervals and New Advances. *IEEE Trans. Neural Netw.* **2011**, *22*, 1341–1356. [[CrossRef](#)] [[PubMed](#)]
22. Huang, G. An Insight into Extreme Learning Machines: Random Neurons, Random Features and Kernels. *Cogn. Comput.* **2014**, *6*, 376–390. [[CrossRef](#)]

23. Li, K.; Qi, X.; Wei, B. Prediction of Transformer Top Oil Temperature Based on Kernel Extreme Learning Machine Error Prediction and Correction. *High Volt. Eng.* **2017**, *43*, 4045–4053. [[CrossRef](#)]
24. Naseri, F.; Kazemi, Z.; Arefi, M. Fast Discrimination of Transformer Magnetizing Current from Internal Faults: An Extended Kalman Filter-Based Approach. *IEEE Trans. Power Deliv.* **2017**, *33*, 110–118. [[CrossRef](#)]
25. Singh, A.K.; Pal, B.C. Rate of Change of Frequency Estimation for Power Systems Using Interpolated DFT and Kalman Filter. *IEEE Trans. Power Syst.* **2019**, *34*, 2509–2517. [[CrossRef](#)]
26. Zhou, L. A Method for Hot-Spot Temperature Prediction and Thermal Capacity Estimation for Traction Transformers in High-Speed Railway Based on Genetic Programming. *IEEE Trans. Transp. Electrification*. **2019**, *5*, 1319–1328. [[CrossRef](#)]
27. Zhao, W.; Tao, T.; Ding, Z. A dynamic particle filter-support vector regression method for reliability prediction. *Reliab. Eng. Syst. Saf.* **2013**, *119*, 109–116. [[CrossRef](#)]
28. Pai, P. System reliability forecasting by support vector machines with genetic algorithms. *Math. Comput. Model.* **2006**, *43*, 262–274. [[CrossRef](#)]
29. Lins, I.D. A Particle Swarm-optimized Support Vector Machine for Reliability Prediction. *Qual. Reliab. Eng. Int.* **2012**, *28*, 141–158. [[CrossRef](#)]